Monomer diffusion rates in photopolymer material. Part I. Low spatial frequency holographic gratings

C. E. Close, M. R. Gleeson, and J. T. Sheridan*

Communications and Optoelectronic Research Centre, SFI Strategic Research Centre in Solar Energy Conversion, School of Electrical, Electronic and Communications Engineering, College of Engineering, Mathematical and Physical Sciences, University College Dublin, Belfield, Dublin 4, Ireland
**Corresponding author: john.sheridan@ucd.ie*

Received October 12, 2010; revised December 21, 2010; accepted December 24, 2010;
posted January 5, 2011 (Doc. ID 136413); published March 9, 2011

For photopolymers, knowing the rate of diffusion of the active monomer is important when modeling the material evolution during recording in order to understand and optimize their performance. Unfortunately, a confusingly wide range of values have been reported in the literature. Re-examining these results, experiments are carried out for both coverplated (sealed) and uncoverplated material layers and the measurements are analyzed using appropriate models. In this way, a more detailed analysis of the diffraction processes taking place for large-period gratings is provided. These results, combined with those in Part II, provide unambiguous evidence that the monomer diffusion rate in a commonly used acrylamide polyvinyl alcohol-based material is of the order of $10^{-10}\,\mathrm{cm}^2/\mathrm{s}$. This value closely agrees with the predictions of the nonlocal polymerization-driven diffusion model.

OCIS codes: 090.0090, 050.2770, 050.7330, 160.5470, 090.2900.

1. INTRODUCTION

Photopolymer materials, as a class of materials, have repeatedly been shown to be effective optical recording media with applications in the areas of holographic data storage [1], surface relief photo-embossing [2], diffractive and refractive optical elements [3], solar concentrators [4], self-focusing beams [5], and hybrid optoelectronic three-dimensional circuitry [6]. Photopolymers are inhomogenous organic materials of various formulations, in which many photochemical and mass transport processes take place both during and postexposure [7–10], resulting in refractive index variations and, thus, diffractive effects. Understanding these processes is critical in developing a model to describe and characterize these materials [11,12]. Further detailed discussion of the polymerisation processes in the material studied here can be found in [7–10].

In an effort to predict the behavior of such materials, much work has been carried out in the development of the nonlocal photopolymerisation-driven diffusion (NPDD) model [13–18]. Achieving good fits to experimental data sets using the NPDD involves fitting by performing searches over fixed ranges for many parameters. The resulting best fits then provide estimates of the parameters' actual physical values. In order to validate the NPDD model, the actual values of these material parameters within the active layer must then be independently determined.

Monomer diffusion plays an important role during photopolymerisation. Therefore, unambiguously establishing a value for the rate of monomer diffusion in the dry material layer is important. Results involving studies using acrylamide/polyvinyl alcohol (AA/PVA), reported by a number of independent research groups, have provided a wide range of diffusion values, estimated using a number of methods [19,20]. Significantly, many of these disagree by factors of ~1000 from the values predicted by the NPDD. Toal *et al.* [19,20], using AA/PVA layers of different thicknesses, estimated the rate of AA diffusion D_{AA} to be 10^{-7}–$10^{-8}\,\mathrm{cm}^2/\mathrm{s}$, while Gallego *et al.* estimated a diffusion constant value of $\sim 10^{-8}\,\mathrm{cm}^2/\mathrm{s}$ [21,22]. We note that, in this paper, we apply a similar experimental approach to that used in [21].

Lawrence *et al.* [14], applying an early version of the NPDD in 2001, estimated values of $D_{\mathrm{AA}} \sim 10^{-14}\,\mathrm{cm}^2/\mathrm{s}$. However, in [14], the rate of diffusion always appeared divided by the rate of polymerization, i.e., the value was extracted from a single lumped parameter and, thus, was not unambiguously estimated. In 2005, Blaya *et al.* [23] reviewed the previous literature and estimated $D_{\mathrm{AA}} \sim 10^{-14}\,\mathrm{cm}^2/\mathrm{s}$. They also noted that the experimental temperature, relative to the material glass transition temperature [24–26], and the matrix composition (molecular weight distribution) [27–29] play very critical roles in determining D_{AA}. However, Blaya *et al.* stated that D_{AA} values of the order of $10^{-7}\,\mathrm{cm}^2/\mathrm{s}$ are not justifiable. Since 2002, Sheridan *et al.*, in a series of papers applying the NPDD model, have consistently estimated D_{AA} to be of the order of $10^{-10}\,\mathrm{cm}^2/\mathrm{s}$ [14–16].

Recently, a physical interpretation of an AA/PVA-based material, which assumes $D_{\mathrm{AA}} \sim 10^{-8}\,\mathrm{cm}^2/\mathrm{s}$ has been presented [30]. This model differs significantly from that of the NPDD model. Clearly, values of $D_{\mathrm{AA}} \sim 10^{-7}$–$10^{-8}\,\mathrm{cm}^2/\mathrm{s}$, or indeed of $10^{-14}\,\mathrm{cm}^2/\mathrm{s}$, call fundamentally into question the validity of the NPDD-based description of free radical photopolymerization.

This paper is the first in a series examining mass transport effects in AA/PVA. In this paper, the experimental method proposed by Gallego *et al.* [21] is employed. Mass transfer effects have been previously examined optically [13]. The most significant difference between the experiments presented here, in Part I, and those in [13], is the size of the period of the gratings examined. In [13], the period examined was $\sim 1\,\mu\mathrm{m}$; here, the large periods examined are $\Lambda \approx \{74, 148, 311\}\,\mu\mathrm{m}$.

Part I is organized as follows. In Section 2, the experimental procedure is outlined. The analytical method applied to interpret the experimental results and the theoretical model of low spatial frequencies grating diffraction is described in Section 3. The results are presented and examined in Section 4. These results are shown to support the predictions of the NPDD model. Section 5 discusses the fitting procedure and Section 6 contains some concluding remarks.

In Part II [31], the results of a different set of experiments, performed to further clarify the value of the diffusion rate, are presented. We believe such detailed study is necessitated by the current confusion in the literature.

2. EXPERIMENT

In all the experiments reported, large-period sinusoidal exposure patterns are generated using a Michelson-type interferometer arrangement (see Fig. 1). This pattern is incident on the AA/PVA material layer and a low spatial frequency grating is recorded. Following the method used in [21], the intensities of the zeroth and first orders diffracted by the grating are monitored, and the rate of grating decay postexposure is related to the rate of diffusion of the monomer in the material. The gratings are all recorded using a solid-state laser of wavelength 532 nm. The material is sensitized to this wavelength using Erythrosin B dye [32]. Further detailed information on the material development, chemical composition, and preparation can be found in [33,34]. Layer thicknesses are typically $d \sim 90\,\mu$m. It should be noted that the PVA matrix used in this study contains molecular weights 30,000–70,000 u. Gallego *et al.* reported experiments carried out using PVA with molecular weights of 27,000 and 150,000 u [21]. Coverplating (sealing) involves the use of silica oil to index match a glass plate (microscope slide) to the material layer. The effects of this are discussed later in more detail.

Returning to the recording setup shown in Fig. 1, we note that the period of the exposing sinusoidal pattern is controlled by a small angle of rotation of the second beam splitter (BS2) and can be measured using a CCD camera (Imperex, IPX-1M48-L). To test the exposing patterns, a ten-period-wide section in each image is selected and, given that the pixel size is 7.4 μm, the period is measured. Figure 2 shows images of the three exposing patterns used.

Having tested the exposing interference patterns, the camera is removed and replaced by the holographic plates as shown in Fig. 1. Gratings are then recorded with a total exposing intensity of 0.4 mW/cm^2. During exposure, the temporal evolution of the grating strength is monitored using a probe

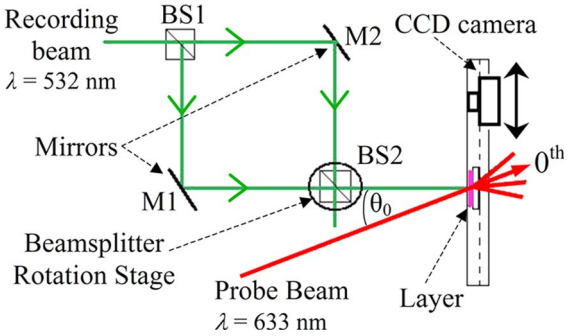

Fig. 1. (Color online) Setup for adjusting period and recording grating.

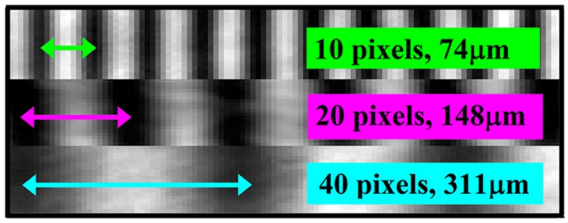

Fig. 2. (Color online) Images taken with the CCD camera of the recording patterns, $\Lambda = \{74, 148, 311\}\,\mu$m.

He–Ne laser of wavelength $\lambda = 633$ nm, to which the dye is insensitive [35]. Significantly, the experiment was carried out for both covered (sealed) and uncovered layers and for different exposure durations.

3. THEORY

Later in this section, we discuss the modeling of postexposure diffusion effects in the layer. However, we begin by noting that the presence of coverplating can have a very significant impact on the measured diffraction efficiency from holographically exposed AA/PVA photopolymer. The presence of coverplating can provide mechanical support and alter surface tension (energy) effects so as to change the profile of the surface relief grating formed during exposure [36,37]. Index matching using silica oil, as part of the coverplating, will significantly reduce the optical effect of any surface relief pattern [38]. Furthermore, in the absence of coverplating, the layer and surface relief profile modulation can be more strongly affected by the environment. For example, shrinkage can occur in the illuminated regions as the water in the layer is heated and evaporates. Such heating will increase due to exothermal polymerization processes [39]. Swelling can occur postexposure, once cooling takes place, as without coverplating water is reabsorbed from the air by the layer, which now contains hydrophillic polyacrylamide (PA) [40].

In this paper, we do not examine the material effects listed above in detail. We do, however, differentiate between the case when, due to coverplating, the optical effects of any surface relief grating are minimized and the case when, in the absence of coverplating, stronger surface grating diffraction takes place. For the purposes of our discussion, Case I refers to the situation where a cover plate is present, and, thus, we only assume the presence of a diffracting refractive index modulation inside the layer, as in Fig. 3. Case II refers to the situation where no coverplating is present, and, thus, both an index and a surface relief grating are simultaneously present during replay, as illustrated in Fig. 4.

The question then arises: how are these two gratings positioned relative to the exposing pattern and one another? When the AA/PVA photopolymer is exposed, shrinkage is initially observed to rapidly take place in illuminated regions [41]. Comparing the surface relief and refractive index gratings, we note that, during exposure and immediately postexposure, the maximum value of index modulation in the layer is colocated at the position of the minimum surface profile height. Therefore, the two gratings are exactly π radians out of phase. This is very significant when examining the cumulative diffraction effect of the two stacked gratings. Analogous effects have previously been studied and reported in the literature [42,43].

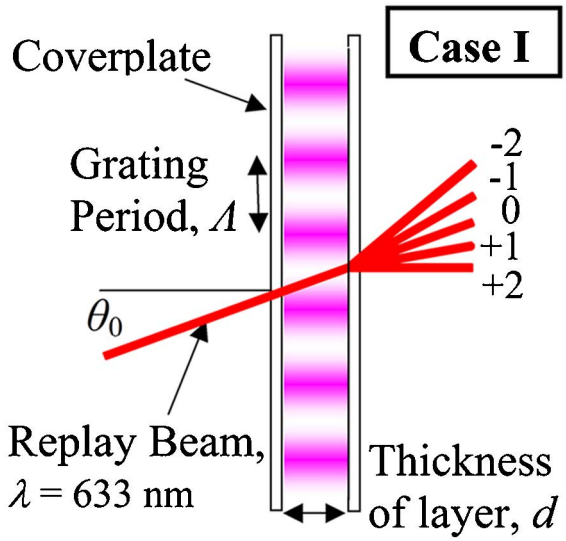

Fig. 3. (Color online) Case I: replay of the index variation grating only.

Diffraction gratings, both holographic and surface relief, are typically described as scattering light in one of two limiting regimes: the Raman–Nath, or thin, regime and the Bragg, or volume or thick, regime [44]. Depending on the diffraction regime, different numbers of diffraction orders contain appreciable amounts of diffracted light. The regime to which a holographic grating belongs can be identified using the thickness parameter, ρ,

$$\rho = \frac{\lambda^2}{\Lambda^2 n_{\mathrm{av}} n_m}, \tag{1}$$

where λ is the wavelength of the replay beam, Λ is the grating period, n_{av} is the average refractive index of the layer, and n_m is the refractive index modulation. Operation in the Raman–Nath regime takes place when $\rho \le 1$ and in the Bragg regime when $\rho \gg 1$. Assuming $1 \le n_{\mathrm{av}} \le 1.5$, $n_m < 0.001$, and $\lambda = 633\,\mathrm{nm}$, in order to operate in the Raman–Nath regime, $\Lambda > 16\,\mu\mathrm{m}$. Recording refractive index gratings at $\Lambda \approx \{74, 148, 311\}\,\mu\mathrm{m}$ gives $\rho = \{0.048, 0.012, 0.002\}$, ensuring operation in the Raman–Nath regime and that many diffraction orders of low diffraction efficiency are produced. Using the grating equation, Eq. (2), we can predict how many diffraction orders are present for a given grating period:

$$\sin\theta_i = \sin\theta_0 + i\lambda/\Lambda. \tag{2}$$

If $\theta_0 \approx 0$, then $|i| \le \{117, 234, 491\}$ for the periods listed above. The grating equation also holds for the surface relief grating. Rigorous electromagnetic theory has been applied to study surface relief structures on volume gratings [45–47]. However, for the large periods and surface amplitudes discussed, i.e., $h < 2\lambda$, the surface phase gratings will also act as thin gratings [48]. Therefore, both gratings can be well approximated using transmittance theory [44,49].

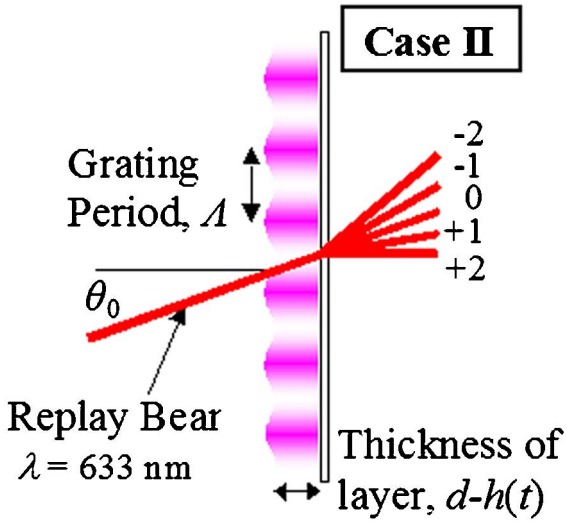

Fig. 4. (Color online) Case II: simultaneous replay of the index variation and the surface relief gratings.

A. Modeling Transmittance: Case I—Coverplated

As previously stated, in this case, it is assumed that only the index modulation, inside the layer, diffracts a significant amount of light. Therefore, it is assumed that the replay beam passes through a single thin unslanted lossless (phase) transmission grating. To model this grating, we introduce a number of physical parameters and employ transmittance theory [44,49]. Given that d is the layer thickness, the transmittance function, $T_m(x,t)$, of the index modulation grating is

$$T_m(x,t) = \exp\left\{+j\frac{2\pi}{\lambda}[n_{\mathrm{av}} + n_m(t)\cos(Kx)]d\right\}, \tag{3}$$

where $n_m(t)$ is the amplitude of the index refractive index modulation, which is a function of time, t. Rewritten as a Fourier series,

$$T_m(x,t) = \exp\left\{+j\frac{2\pi n_{\mathrm{av}} d}{\lambda}\right\} \times \sum_{i=-N}^{+N} J_i[\mu_m(t)]\exp(+jnKx), \tag{4}$$

where

$$\mu_m(t) = \frac{-2\pi n_m(t) d}{\lambda}. \tag{5}$$

Based on Eq. (4) and assuming normally incident plane wave illumination of intensity I_{in}, the predicted diffraction efficiencies of the $i = (0, \pm 1)$ orders are

$$\eta^I_{i,m}(t) = \frac{I^I_{i,m}}{I_{in}} = |J_i[\mu_m(t)]|^2, \tag{6}$$

where $I^I_{i,m}$ is the intensity of the ith diffracted order at a small angle, $\theta_i \sim i\lambda/\Lambda\,\mathrm{rad}$, for Case I.

B. Modeling Transmittance: Case II—Uncoverplated

When the index modulation grating is being formed, PA is generated in the bright regions. This leads to rapid surface shrinkage, since PA takes up less space than the corresponding AA [50]. As noted, localized heating may lead to some evaporation of water, and the PA formed is a hydrophilic material [40]. This means that postexposure water molecules from the environment diffuse into the layer. Furthermore, AA diffuses in from the unexposed regions in the layer into the exposed

regions. Therefore, postexposure, the exposed regions swell slowly. The resulting shrinkage followed by swelling leads to the formation of a surface relief grating with the same period size as the index modulation grating [36,37].

However, in Case II, both a thin index modulation and a thin surface relief grating are simultaneously formed and diffract light. The transmittance function of the surface relief grating $T_S(x,t)$ is given by

$$T_S(x,t) = \exp\left\{+j\frac{2\pi(n_{\text{av}}+n_a)h(t)}{2\lambda}\right\} \times \exp\left\{+j\frac{2\pi(n_{\text{av}}-n_a)h(t)}{2\lambda}\cos(Kx)\right\}, \quad (7)$$

where $h(t)$ is the time-varying height of the l surface relief grating and the refractive index of air, $n_a = 1$. Multiplying $T_m(x,t)$, Eq. (3), by $T_s(x,t)$, Eq. (7), gives the composite transmittance of the two thin gratings:

$$T_{\text{Tot}}(x,t) = \exp\left\{+j\frac{2\pi[2n_{\text{av}}(t)[d-h(t)]+(n_{\text{av}}+n_a)h(t)]}{2\lambda}\right\} \times \exp\{+j\mu_{\text{Tot}}(t)\cos(Kx)\}, \quad (8)$$

where

$$\mu_{\text{Tot}}(t) = \frac{\pi}{\lambda}\{-2n_m(t)[d-h(t)]+(n_{\text{av}}-n_a)h(t)\}. \quad (9)$$

We note that, in all cases examined in this paper, $h(t) \ll d$ and $n_m(t) \ll n_{\text{av}}$. Taking the Fourier transform of Eq. (8) allows us to express the output field as a sum of the amplitudes of the individual components [42],

$$T_{\text{Tot}}(x,t) = \exp\left\{+j\frac{2\pi[2n_{\text{av}}[d-h(t)]+(n_{\text{av}}+n_a)h(t)]}{2\lambda}\right\} \times \sum_{i=-N}^{+N} J_i[\mu_{\text{Tot}}(t)]\exp(+jKx). \quad (10)$$

For an incident plane wave of intensity I_{in}, the predicted diffraction efficiency of the $i = (0, \pm 1)$ diffraction orders are

$$\eta_{i,\text{Tot}}(t) = \left[\frac{I^{\text{II}}_{i,\text{Tot}}}{I_{\text{in}}}\right] = \{J_i[\mu_{\text{Tot}}(t)]\}^2, \quad (11)$$

where $I^{\text{II}}_{i,\text{Tot}}$ is the diffracted intensity at $\theta_i \sim i\lambda/\Lambda$ rad, for Case II. Applying Eq. (11), in Fig. 5, we examine the predicted behavior of the zeroth diffraction order for a range of refractive index modulation amplitudes and surface relief profile heights. It can be clearly seen that the surface grating is predicted to have a very appreciable impact on the amount of light diffracted from the zeroth order. Significantly, we note the existence of a set of combinations of n_m and h values for which no light is diffracted. This is indicated in the figure by the presence of the thick dashed line. The thick solid line in Fig. 5, when $h = 0$, indicates the expected behavior when it is assumed no diffraction by the surface relief profile takes place (i.e., in the perfectly coverplated case).

In this section, a model, describing diffraction by the two types of grating present, is developed. However, before discussing experimental results, some analysis of the mass transport effects taking place in the layer is necessary.

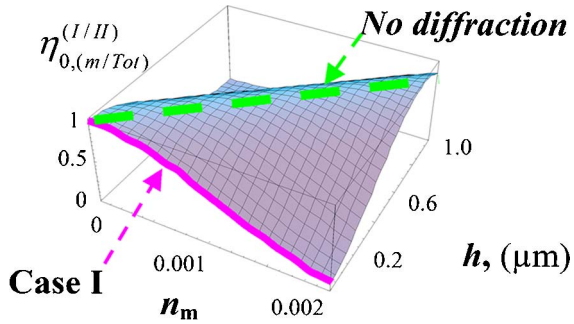

Fig. 5. (Color online) Cases I and II: the zeroth-order diffraction efficiencies plotted as a function of the index modulation, n_m, and surface relief grating height, h. Dashed line indicates where, in Case II, no diffraction to higher orders occurs. Solid line indicates the Case I evolution of the zeroth order.

C. Postexposure Diffusion

In previous high spatial frequency holographic studies, the postexposure decay of the refractive index modulation of a grating, arising primarily due to the diffusion of uncrosslinked photopolymer, has been discussed [21]. In these studies, it has been shown that the observed decay of the refractive index modulation in the layer, n_m, can be described using

$$n_m(t) = n_m(t\to\infty) + \Delta n_m \exp[-\alpha_m t], \quad (12)$$

where $n_m(t\to\infty)$ is the minimum value of the refractive index modulation below which the grating does not decay further under controlled conditions. α_m is the decay constant of the grating refractive index modulation and Δn_m is the observed modulation index variation. An approximate value for $n_m(t\to\infty)$ is found by assuming that a long time postexposure, the refractive index modulation reaches a steady state, and so the last measured value at $t = t_{\text{final}}$ is equivalent to the value at $t\to\infty$. Thus, $n_m(t\to\infty) \approx n_m(t_{\text{final}})$. Combining this assumption and Eq. (12) gives

$$\ln[n_m(t) - n_m(t_{\text{final}})] = \ln[\Delta n_m] - \alpha_m t, \quad (13)$$

and the slope of this line, α_m, is the rate of decay of the grating index modulation.

In this case, the postexposure decay of the modulation is diffusion driven, and is governed by Fick's first law [51,52]:

$$\frac{\partial C(x,t)}{\partial t} = D_m\frac{\partial^2 C(x,t)}{\partial x^2}, \quad (14)$$

where $C(x,t)$ is the concentration of the diffusing substance at time t and position x, and D_m is the rate of diffusion of the material forming the concentration modulation. D_m is assumed to be constant at all times throughout the medium. Solving Eq. (14) requires the application of two boundary conditions and one initial condition. We begin by assuming that, when $t = 0$,

$$C(x,0) = C_{\text{AV}} + C_a\cos[Kx], \quad (15)$$

where $K = 2\pi/\Lambda$ is the grating vector magnitude with Λ the grating period of the interference pattern recorded, C_{AV} is the

average concentration of material free to diffuse, while C_a is the maximum amplitude of the concentration of AA that is not rigidly held in place. The concentration function must have a finite value for all values of x and t, i.e., $C(x,t) \geq 0$, and, furthermore, $C(x, t \to \infty) = C_{\mathrm{AV}}$. Therefore,

$$\frac{1}{\Lambda}\int_0^{\Lambda} C(x,t)\mathrm{d}t = C_{\mathrm{AV}}. \tag{16}$$

Applying these conditions, the solution to Eq. (14) is given by

$$C(x,t) = C_{\mathrm{AV}} + C_a \exp\left[-D_m\left(\frac{2\pi}{\Lambda}\right)^2 t\right]\cos\left[\frac{2\pi x}{\Lambda}\right]. \tag{17}$$

Let us assume that the refractive index modulation is linearly proportional to the polymer concentration, $C(x,t)$, within the material [13]. Returning to Eq. (12), we can then state that

$$\Delta n_m \exp[-\alpha_m t] \propto C_a \exp\left[-D_m\left(\frac{2\pi}{\Lambda}\right)^2 t\right], \tag{18}$$

which implies that

$$\alpha_m = D_m K^2 = D_m\left(\frac{2\pi}{\Lambda}\right)^2. \tag{19}$$

Thus, the rate of diffusion and the decay constant of the grating are linearly related. This form of diffusion analysis is applied later in Subsection 4.B and again in Part II [31].

4. EXPERIMENTAL RESULTS

In this section, experiments performed, both during and postexposure, are presented.

A. During Exposure

We first examine grating evolution during exposure. Inhibition periods (dead bands) play a significant role in the initial stages of hologram formation [53] and, in the experiments reported here, have been observed to last up to ~8 s depending on the size of the grating period and the presence of coverplating. During this inhibition period, exposure takes place, but no grating is formed. To simplify the analysis, the graphs presented have been shifted so that the end of the inhibition period [53] and, thus, the beginning of grating diffraction occurs at $t = 0$ s. Figure 6 shows the evolution of the zeroth and first diffraction orders during recording for both Cases I and II when $\Lambda \approx 148\,\mu$m. As expected, the amount of light diffracted by the uncoverplated grating increases more slowly as the surface relief grating scatters out of phase with the index modulation grating, reducing the combined diffraction effects.

Applying the theory presented in Subsection 3.A to process the measured experimental data, the argument of the Bessel function $\mu_m(t)$, Eq. (5) is extracted, and these results are shown in Fig. 7. We note that the differences between the pairs of curves for Cases I and II can be explained by the diffraction by the surface height variation, $h(t)$, arising due to the evolution of the surface relief profile.

B. Postexposure

We now examine the experimental results obtained postexposure and compare them to the predictions of our model. We begin by noting that the diffusion rate of the PA, D_{PA}, in cross-linked AA/PVA has been shown to be of the order of 10^{-15} cm^2/s [13,32]. Therefore, following [21], we neglect PA diffusion. Thus, any decay of n_m is assumed to arise solely due to monomer diffusion [20,21]. We also note that some continued polymer chain growth postexposure has been observed and analyzed in the literature [8,17], but is neglected here.

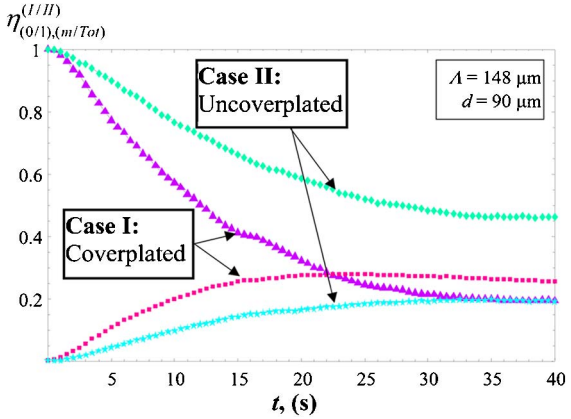

Fig. 6. (Color online) Evolution of the zeroth and first diffraction orders for Cases I and II where the recording intensity is 0.4 mW/cm^2.

As previously mentioned, experiments were carried out for a number of different periods. Figure 7 shows the postexposure evolution of the zeroth order for both Cases I and II and a period of $\Lambda = 148\,\mu$m. In both cases, the zeroth-order intensities are observed to decrease during exposure, although at different rates. However, their postexposure behavior is very different. Taking the natural logarithm of the change in diffraction efficiencies, the inset graph in Fig. 8 is obtained. It was previously shown, in Subsection 3.C, that the slopes of the graphs in Fig. 8 are proportional to the rate of diffusion of the material, which alters the modulation, i.e., n_m. It is clear from Fig. 8 that the observed slope in the presence of coverplating, Case I, is significantly smaller than that for Case II when the grating is not coverplated.

The results shown in Fig. 9 are for grating periods of $\Lambda \sim 311\,\mu$m. The graph shows the logarithm of the refractive index variation for the first diffracted order. For Case I (coverplated), the grating decays linearly as a result of the diffusion of the monomer from the unexposed to the exposed regions. In Case II (uncoverplated), the grating decays at a

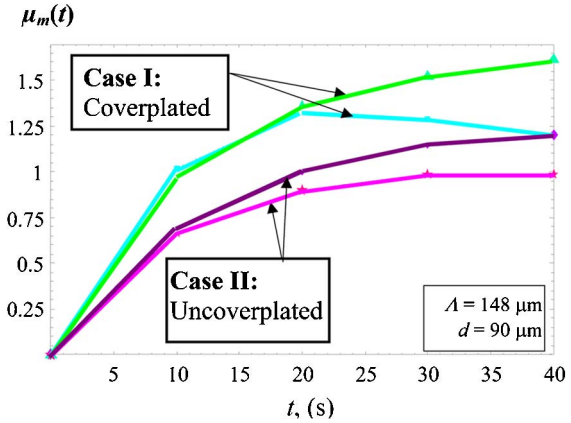

Fig. 7. (Color online) Arguments of the Bessel function $\mu_i(t)$ for zeroth and first order for Cases I and II, where the recording intensity is 0.4 mW/cm^2

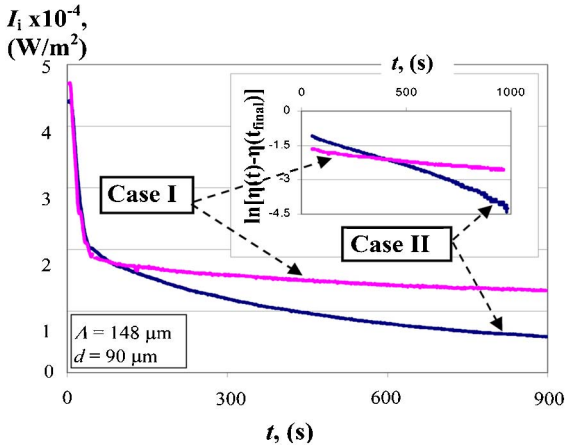

Fig. 8. (Color online) Evolution of zeroth order for Cases I and II with a recording intensity of 0.4 mW/cm^2 with the corresponding natural logarithm of $[\eta(t) - \eta(t_{\text{final}})]$ shown in the inset.

significantly faster rate as shrinkage in the exposed material areas leads to the formation of a surface relief grating out of phase with the index modulation grating, which reduces the combined diffraction effect. Eventually, postexposure, the surface relief grating height starts to decrease, and, as noted, the exposed regions will even eventually swell. In this way, the surface grating eventually comes into phase with the index modulation grating. In Fig. 9, a minimum can be observed in the Case II results when the diffraction effects of the two gratings almost cancel, which is followed by a slow increase. The results presented above are based on many independent measurements made over long periods of time, $0 \le t \le 2000$ s.

5. FITTING PROCEDURE

Having established a theoretical description of the zeroth and first diffraction orders and observed differences in the experimental results obtained for Cases I and II, we now fit the experimental results using the theory in Section 2. First, we extract $\mu_m(t)$ and $\mu_{\text{tot}}(t)$ from the measured diffraction efficiency data, and then describe the evolution of $n_m(t)$ and $h(t)$ by fitting the results using simple analytic expressions.

While $n_m(t)$ can be estimated using the NPDD [15], this is not necessary for our stated objectives. Starting with Case I, i.e., index modulation gratings only, the experimental results were fit using Eqs. (5) and (6). From this fitting procedure, an

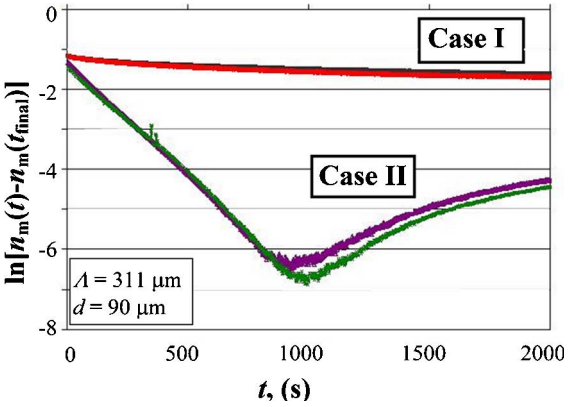

Fig. 9. (Color online) Natural logarithm of $[n_m(t) - n_m(t_{\text{final}})]$ and Case II with a recording intensity of 0.4 mW/cm^2.

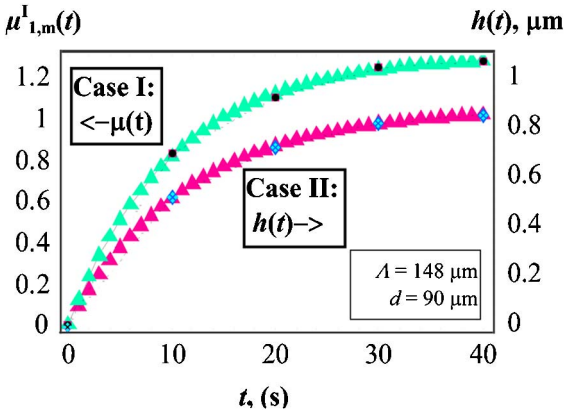

Fig. 10. (Color online) Evolution during exposure of $\mu^{\text{I}}_{1,m}(t)$ for Case I (left axis) and $h(t)$ for Case II (right axis). Triangles indicate the fitted curves, while circles and diamonds indicate experimental results.

expression for the time-varying refractive index modulation, $n_m(t)$, is found. We assume that coverplating leaves the processes inside the layer largely unaffected, i.e., it gives rise to negligible variations in the index modulation formation process. Therefore, the expression found for $n_m(t)$ for Case I can be substituted into Eq. (9) for Case II, leaving the time-varying height, $h(t)$, as the only unknown. Equation (11) can then be fit to the data for the uncovered layers and an expression for $h(t)$ found.

Then, we look at extracting the rate of diffusion of AA and compare the results for the coverplated and uncoverplated cases. It is shown how neglecting to take account of the formation and evolution of the surface relief profile, in the case of uncoverplated layers, results in the extraction of a false too-high value for D_{AA}. The coverplated layers, for which the effects of the surface relief profiles are minimized, thus provide a truer value of the rate of diffusion of AA in the layer.

A. Analyzing the Data

1. Case I—Coverplated during Exposure

The fitting described here is carried out on data for $\Lambda = 148\,\mu$m exposures. Starting with the measured diffraction efficiency curve for the zeroth order (Case I), a set of diffraction efficiency data points, $\eta^I_{0,m}(t)$, as a function of time, were extracted. Using the expression in Eq. (6) for the zeroth-order

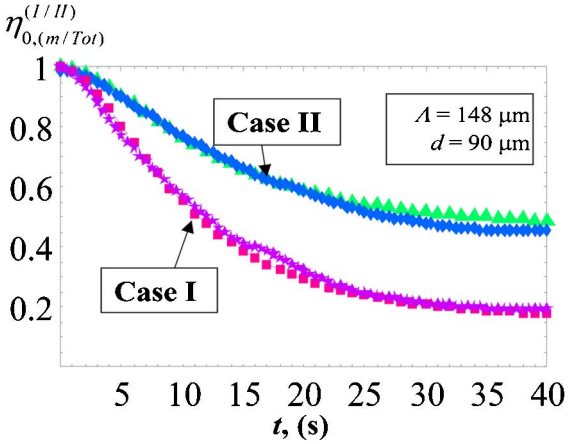

Fig. 11. (Color online) Fits and experiment for zeroth order for Cases I and II. Squares and triangles indicate the fitted curves, while stars and diamonds indicate experimental results.

Table 1. Monomer Diffusion Rates Obtained for Cases I and II for Different Temperatures, Humidities, and Periods[a]

	$T = 20$–$23\,^{\circ}\mathrm{C}$, $RH = 55\%$–65%			$T = 10$–$13\,^{\circ}\mathrm{C}$, $RH = 35\%$–45%		
Λ	$74\,\mu$m	$148\,\mu$m	$311\,\mu$m	$74\,\mu$m	$148\,\mu$m	$311\,\mu$m
Spatial frequency	14 l/mm	7 l/mm	3 l/mm	14 l/mm	7 l/mm	3 l/mm
D_{AA}, cm^2/s,	5.64×10^{-10}	2.26×10^{-8}	5.39×10^{-8}	1.77×10^{-9}	3.83×10^{-9}	1.60×10^{-8}
Case I—covered	$\pm 5.13 \times 10^{-10}$	$\pm 1.64 \times 10^{-8}$	$\pm 2.48 \times 10^{-8}$	$\pm 1.09 \times 10^{-9}$	$\pm 2.86 \times 10^{-9}$	$\pm 0.82 \times 10^{-8}$
Apparent D_{AA}, cm^2/s,	9.29×10^{-9}	3.65×10^{-7}	3.29×10^{-7}	3.61×10^{-9}	9.86×10^{-9}	3.19×10^{-7}
Case II—uncovered	$\pm 2.62 \times 10^{-9}$	$\pm 2.82 \times 10^{-7}$	$\pm 3.09 \times 10^{-7}$	$\pm 2.28 \times 10^{-9}$	$\pm 5.25 \times 10^{-9}$	$\pm 2.53 \times 10^{-7}$

[a]Case II results fail to take into account the surface relief profile and are thus incorrect.

diffraction efficiency, $i = 0$, a corresponding set of points for $\mu_m(t)$ are found. This data is then fit using a simple analytic expression, and a closed form expression for the argument, $\mu_m(t)$, is found. Using Eq. (5) and multiplying across by $\lambda/(-2\pi d)$, the resulting values for $n_m(t)$ are fit using the expression

$$n_m(t) = \delta_m[1 - \exp(-\beta_m t)]. \tag{20}$$

Using Mathematica [54] results in best-fit parameter values $\delta_m = 0.00131$ and $\beta_m = 0.9827$. The data and the resulting best fit appear in Fig. 10. These results are also confirmed for the corresponding $i = \pm 1$ diffraction order data.

2. Case II—Uncoverplated during Exposure

Case II assumes the presence of a diffracting surface relief profile. Following a similar procedure to Case I, a set of values describing $\mu_{\mathrm{Tot}}(t)$ were estimated from diffraction efficiency measurements using Eq. (11) with $i = 0$. The expression obtained for $n_m(t)$ in Eq. (20) is substituted into Eq. (9), and then an analytic expression for $h(t)$ of the form

$$h(t) = \delta_s[1 - \exp(-\beta_s t)] \tag{21}$$

is used. Fitting this to the data, the best-fit parameter values found are $\delta_s = 9.967 \times 10^{-7}$ and $\beta_s = 0.0965$ [54]. The resulting best fit is presented along with the corresponding data in Fig. 10. No theoretical basis or further explanation for either Eqs. (20) or (21) is given here, as it is beyond the scope of this paper.

Figure 11 contains data and fits to the experimental data for both Cases I and II. It is clear that completely neglecting the effects of the surface relief grating height variation when analyzing the experimental data leads to very significant errors.

B. Estimating Monomer Diffusion Postexposure

In Subsection 3.C, the approach used to find a value for AA diffusion is discussed. The value of the rate of decay of the grating, α_M, is substituted into Eq. (19) to find a value for the rate of diffusion, D_{AA}. The results for Cases I and II for each of the three periods examined are presented in Table 1. However, as noted, both temperature and humidity also play a significant role in diffusion processes. Experiments for different ambient conditions, i.e., temperatures and humidities, were also performed, and the results are reported in Table 1.

Higher temperature results in the polymer layer being closer to its glass transition temperature, T_g, and, therefore, mass transport within the layer can more freely take place, i.e., the viscosity is lower. Higher relative humidity, RH, can result in more water in the layer and, therefore, lower density and viscosity. Therefore, the layer is more sensitive to environmental changes if no coverplating is present. Furthermore, in the absence of coverplating, surface roughness can also degrade optical performance; therefore, the experimental results are less consistent (i.e., less reproducible) than in the coverplated case. Thus, the absence of coverplating significantly affects the estimated rate of diffusion using this method. Examining the results in Table 1 and taking into account the effect of temperature, humidity, and the surface relief profile leads to the conclusion that the values for the rate of diffusion estimated using uncoverplated layers are incorrect, while those found using the results for the coverplated material are closer to the true rate of diffusion of monomer in the layer.

Examining Table 1, it is clear that, in all cases, the estimated D_{AA} values obtained for the uncoverplated material is higher than for the coverplated layers. This is as expected, based on our description of the effects of the surface relief gratings. We also note that, in general, as the period increases, the predicted rates of diffusion also increase. This can be explained in terms of the effect of surface tension on the formation of the surface profile. For larger periods, the height variations are larger and take place more rapidly due to the lower energy restriction imposed by the lower surface curvatures in these profiles. Since perfect index matching cannot be achieved, the surface relief grating still has an effect on the Case I results. Significantly, however, as the period decreases and, thus, the surface relief pattern is more constrained, the diffusion rates decrease in the coverplated cases toward $\sim 10^{-10}\,\mathrm{cm}^2/\mathrm{s}$, indicating a maximum possible value.

In summary, (1) uncoverplated versus coverplated, $D_{\mathrm{AA}}(\mathrm{Case\ II}) > D_{\mathrm{AA}}(\mathrm{Case\ I})$; and (2) periods, $D_{\mathrm{AA}}(\Lambda_1) > D_{\mathrm{AA}}(\Lambda_2)$ when $\Lambda_1 > \Lambda_2$.

6. CONCLUSIONS

Recent results have been reported in the literature, predicting extremely fast and extremely slow rates of diffusion of AA monomer in a PVA matrix, i.e., $D_{\mathrm{AA}} \sim 10^{-7}$–$10^{-8}\,\mathrm{cm}^2/\mathrm{s}$ [19–21] and $D_{\mathrm{AA}} \sim 10^{-14}\,\mathrm{cm}^2/\mathrm{s}$ [15,24]. Such a wide range of values are confusing and conflict with the predictions of the NPDD model.

The experimental results reported here are based on measured data produced following the procedure in [21]. They unambiguously indicate that previously [19–22] a critically important physical effect, namely, diffraction by the surface relief grating induced during exposure, is neglected. Using the methodology described here, rates of monomer diffusion

$D_{AA} \sim 10^{-9}\,\mathrm{cm}^2/\mathrm{s}$ have been repeatedly extracted under a variety of exposure and environmental conditions. This value is significantly slower than those reported in [19–22], but faster than those reported in [23]. Furthermore, we note that the actual value of D_{AA} will be slower than the values estimated here since the coverplating method employed is not perfect and the smallest period size is still large enough to be accompanied by significant surface changes. Optically, since exact index matching is not achieved, some diffraction by the surface relief grating takes place, which still acts against the effect of the modulation grating, reducing the diffraction efficiency of the $\pm$1st orders. Clearly, further study is necessary.

In Part II, a lower bound for the rate of monomer diffusion is estimated, and further investigations into the upper bound value are performed. These studies are carried out using different experimental methods and the overall consistency of the reported results provides evidence supporting the validity of the NPDD model estimate of D_{AA} being in the range 10^{-11}–$10^{-10}\,\mathrm{cm}^2/\mathrm{s}$.

It has been brought to our attention that, in a recent paper by Toal *et al.* [55], inappropriate initial monomer and polymer diffusion values ($D_m \sim D_{0m} = 5 \times 10^{-11}\,\mathrm{m}^2\mathrm{s}^{-1} = 5 \times 10^{-7}\,\mathrm{cm}^2\mathrm{s}^{-1}$ and $D_p \sim D_{0p} = 1.2 \times 10^{-12}\,\mathrm{m}^2\mathrm{s}^{-1} = 1.2 \times 10^{-8}\,\mathrm{cm}^2\mathrm{s}^{-1}$) have been employed to discuss a similar AA/PVA-type material.

ACKNOWLEDGMENTS

We acknowledge the support of Enterprise Ireland, Science Foundation Ireland as part of the National Development Plan and the Irish Research Council for Science, Engineering and Technology.

REFERENCES

1. J. Ashley, M. P. Bernal, G. W. Burr, H. Coufal, H. Guenther, J. A. Hoffnagle, C. M. Jefferson, B. Marcus, R. M. MacFarlane, R. M. Shelby, and G. T. Sincerbox, "Holographic data storage technology," IBM J. Res. Dev. **44**, 341–368 (2000).
2. F. T. O'Neill, A. J. Carr, S. M. Daniels, M. R. Gleeson, J. V. Kelly, J. R. Lawrence, and J. T. Sheridan, "Refractive elements produced in photopolymer layers," J. Mater. Sci. **40**, 4129–4132 (2005).
3. G. P. Nordinand and A. R. Tanguay, Jr., "Photopolymer-based stratified volume holographic optical elements," Opt. Lett. **17**, 1709–1711 (1992).
4. R. K. Kostuk, J. Castro, and D. Zhang, "Holographic low concentration ratio solar concentrators," in *Frontiers in Optics*, OSA Technical Digest (CD) (Optical Society of America, 2009), paper FMB3.
5. J. Zhang, K. Kasala, A. Rewari, and K. Saravanamuttu, "Self-trapping of spatially and temporally incoherent white light in a photochemical medium," J. Am. Chem. Soc. **128**, 406–407 (2006).
6. A. C. Sullivan, M. W. Grabowski, and R. R. McLeod, "Three-dimensional direct-write lithography into photopolymer," Appl. Opt. **46**, 295–301 (2007).
7. M. R. Gleeson, J. V. Kelly, D. Sabol, C. E. Close, S. Lui, and J. T. Sheridan, "Modelling the photochemical effects present during holographic grating formation in photopolymer materials," J. Appl. Phys. **102**, 023108 (2007).
8. M. R. Gleeson and J. T. Sheridan, "Nonlocal photopolymerization kinetics including multiple termination mechanisms and dark reactions. Part I. Modelling," J. Opt. Soc. Am. B **26**, 1736–1745 (2009).
9. M. R. Gleeson, S. Liu, R. R. McLeod, and J. T. Sheridan, "Nonlocal photopolymerization kinetics including multiple termination mechanisms and dark reactions. Part II. Experimental validation," J. Opt. Soc. Am. B **26**, 1746–1754 (2009).
10. S. Liu, M. R. Gleeson, J. Guo, and J. T. Sheridan, "High intensity response of photopolymer materials for holographic grating formation," Macromolecules **43**, 9462–9472 (2010).
11. G. Zhao and P. Mouroulis, "Diffusion model of hologram formation in dry photopolymer materials," J. Mod. Opt. **41**, 1929–1939 (1994).
12. J. T. Sheridan and J. R. Lawrence, "Nonlocal-response diffusion model of holographic recording in photopolymer," J. Opt. Soc. Am. A **17**, 1108–1114 (2000).
13. F. T. O'Neill, J. R. Lawrence, and J. T. Sheridan, "Improvement of holographic recording material using aerosol sealant," J. Opt. A: Pure Appl. Opt. **3**, 20–25 (2001).
14. J. R. Lawrence, F. T. O'Neill, and J. T. Sheridan, "Adjusted intensity non-local diffusion model of photopolymer grating formation," J. Opt. Soc. Am. B **19**, 621–629 (2002).
15. F. T. O'Neill, J. R. Lawrence, and J. T. Sheridan, "Comparison of holographic photopolymer materials by use of analytic non-local diffusion models," Appl. Opt. **41**, 845–852 (2002).
16. J. V. Kelly, M. R. Gleeson, C. E. Close, F. T. O'Neill, J. T. Sheridan, S. Gallego, and C. Niepp, "Temporal analysis of grating formation in photopolymer using the nonlocal polymerisation-driven diffusion model," Opt. Express **13**, 6990–7004 (2005).
17. J. V. Kelly, F. T. O'Neill, J. T. Sheridan, C. Neipp, S. Gallego, and M. Ortuno, "Holographic photopolymer materials: nonlocal polymerisation-driven diffusion under nonideal kinetic conditions," J. Opt. Soc. Am. B **22**, 407–416 (2005).
18. J. T. Sheridan, M. R. Gleeson, C. E. Close, and J. V. Kelly, "Optical response of photopolymer materials for holographic data storage applications," J. Nanosci. Nanotech. **7**, 232–242 (2007).
19. I. Naydenova, R. Jallapuram, R. Howard, S. Martin, and V. Toal, "Investigation of the diffusion processes in a self-processing acrylamide-based photopolymer system," Appl. Opt. **43**, 2900–2905 (2004).
20. T. Babeva, I. Naydenova, S. Martin, and V. Toal, "Method for characterization of diffusion properties of photopolymerisable systems," Opt. Express **16**, 8487–8497 (2008).
21. S. Gallego, A. Marquez, D. Mendez, C. Neipp, M. Ortuno, A. Belendez, E. Fernandez, and I. Pascual, "Direct analysis of monomer diffusion times in polyvinyl/acrylamide materials," Appl. Phys. Lett. **92**, 073306 (2008).
22. S. Gallego, A. Marquez, S. Marini, E. Fernandez, M. Ortuno, and I. Parcual, "In dark analysis of PVA/AA materials at very low spatial frequencies: phase modulation evolution and diffusion estimation," Opt. Express **17**, 18279–19291 (2009).
23. S. Blaya, L. Carretero, P. Acebal, R. F. Madrigal, A. Murciano, M. Ulibarrena, and A. Fimia, "Analysis of the diffusion processes in dry photopolymerizable holographic recording materials," Proc. SPIE**5827**, 128–139 (2005).
24. M. Antonietti, J. Coutandin, R. Grtutter, and H. Sillescu, "Diffusion of labeled macromolecules in molten polystyrenes studied by a holographic grating technique," Macromolecules **17**, 798–802 (1984).
25. J. Zhang, C. H. Wang, and D. Ehlich, "Investigation of the mass diffusion of camphorquinone in amorphous poly(methyl methacrylate) and poly(*tert*-butyl-methacrylate) hosts by the induced holographic grating relaxation technique," Macromolecules **19**, 1390–1394 (1986).
26. C. H. Wang and J. L. Xia, "Holographic grating studies of the diffusion process of camphorquinone in polycarbonate above and below *tg*," Macromolecules **21**, 3519–3523 (1988).
27. D. Ehlich and H. Sillescu, "Tracer diffusion at the glass transition," Macromolecules **23**, 1600–1610 (1990).
28. J. Xia and C. H. Wang, "Holographic grating relaxation studies of probe diffusion in a polymer blend," Macromolecules **32**, 5655–5659 (1999).
29. A. V. Veniaminov and H. Sillescu, "Polymer and dye probe diffusion in poly(methyl methacrylate) below the glass transition studied by forced Rayleigh scattering," Macromolecules **32**, 1828–1837 (1999).
30. T. Babeva, I. Naydenova, D. Mackey, S. Martin, and V. Toal, "Two-way diffusion model for short-exposure holographic grating formation in acrylamide-based photopolymer," J. Opt. Soc. Am. B **27**, 197–203 (2010).

31. C. E. Close, M. R. Gleeson, D. A. Mooney, and J. T. Sheridan, "Monomer diffusion rates in photopolymer material: part II: high frequency gratings and bulk diffusion," J. Opt. Soc. Am. B, doc. ID 136413 (posted 5 January 2011, in press).
32. S. Liu, M. R. Gleeson, and J. T. Sheridan, "Analysis of the photoabsorptive behavior of two different photosensitisers in a photopolymer material," J. Opt. Soc. Am. B **26**, 528–536 (2009).
33. F. T. O'Neill, J. R. Lawrence, and J. T. Sheridan, "Automated recording and testing of holographic optical element arrays," Optik (Jena) **111**, 459–467 (2000).
34. J. R. Lawrence, F. T. O'Neill, and J. T. Sheridan, "Phtopolymer holographic recording material," Optik (Jena) **112**, 449–463 (2001).
35. P. V. Kamat and M. A. Fox, "Photophysics and photochemistry of xanthene dyes in polymer solutions and films," J. Phys. Chem. **88**, 2297–2302 (1984).
36. L. M. C. Sagis, "Generalised curvature expansion for the surface internal energy," Phys. At. Nucl. **246**, 591–608 (1997).
37. S. Abe and J. T. Sheridan, "Curvature correction model of droplet profiles," Phys. Lett. A **253**, 317–321 (1999).
38. W. S. Colburn and K. A. Haines, "Volume hologram formation in photopolymer materials," Appl. Opt. **10**, 1636–1641 (1971).
39. G. K. Oster, G. Oster, and G. Prati, "Dye-sensitized photopolymerisation of acrylamide," J. Am. Chem. Soc. **79**, 595–598 (1957).
40. S. Mishra, R. Bajpai, R. Katare, and A. K. Bajpai, "Preparation and characterization of polyvinyl alcohol based biomaterials: water sorption and *in vitro* blood compatibility study," J. Appl. Polym. Sci. **100**, 2402–2408 (2006).
41. J. V. Kelly, M. R. Gleeson, C. E. Close, F. T. O'Neill, and J. T. Sheridan, "Temporal response and first order volume changes during grating formation in photopolymers," J. Appl. Phys. **99**, 113105 (2006).
42. J. T. Sheridan, "Stacked volume holographic gratings. Part I. Transmission gratings in series," Optik (Jena) **95**, 73–80 (1993).
43. M. R. Gleeson, J. V. Kelly, F. T. O'Neill, and J. T. Sheridan, "Recording beam modulation during grating formation," Appl. Opt. **44**, 5475–5482 (2005).
44. R. R. A. Syms, *Practical Volume Holography* (Clarendon, 1990).
45. N. Kamiya, "Rigorous coupled wave analysis for practical planar dielectric gratings: 1. Thickness-changed holograms and some characteristics of diffraction efficiency," Appl. Opt. **37**, 5843–5853 (1998).
46. N. Kamiya, "Rigorous coupled wave analysis for practical planar dielectric gratings: 2. Diffraction by a surface-eroded hologram layer," Appl. Opt. **37**, 5854–5863 (1998).
47. N. Kamiya, "Rigorous coupled wave analysis for practical planar dielectric gratings: 3. Increase of higher-order lights owing to degenerated complex diffraction," Appl. Opt. **37**, 5864–5878 (1998).
48. R. Petit, *Electromagnetic Theory of Gratings* (Springer-Verlag, 1980).
49. J. W. Goodman, *Introduction to Fourier Optics* (Roberts & Company, 2005).
50. H. M. Karpov, V. V. Obukhovsky, and T. N. Smirnova, "Generalized model of holographic recording in photopolymer material," Semicond. Phys. Quantum Electron. Optoelectron. **2**, 66–70 (1999).
51. J. Crank, *The Mathematics of Diffusion*, 2nd ed. (Oxford University, 1975).
52. J. Crank and G. S. Park, *Diffusion in Polymers*, 1st ed. (Academic, 1968).
53. M. R. Gleeson, J. V. Kelly, C. E. Close, F. T. O'Neill, and J. T. Sheridan, "The effects of absorption and inhibition during grating formation in photopolymer materials," J. Opt. Soc. Am. B **23**, 2079–2088 (2006).
54. S. Wolfram, "Mathematica," www.wolfram.com/mathematica.
55. T. Babeva, D. Mackey, I. Naydenova, S. Martin, and V. Toal, "Study of the photoinduced surface relief modulation in photopolymers caused by illumination with a Gaussian beam of light," J. Opt. **12**, 124011 (2010).